Optimizing Dynamic Legged Locomotion in Mixed, Resistive Media

Max Austin[1], John Nicholson[2], Jason White[1], Sean Gart[2],
Ashley Chase[1], Jason Pusey[2], Christian Hubicki[1] and Jonathan E. Clark[1]

***Abstract*— Locomotion through resistive media is an organic occurrence during traversal of the natural world. Due to the complexities required to analyze the effect of these media on the dynamics of locomotion, controllers of legged robots generally neglect or treat them as disturbances. In this paper, we address the challenge of producing optimal locomotion control in resistive media. We do so by applying trajectory optimization techniques within a direct collocation framework onto a reduced-order resistive model of legged locomotion: the Fluid Field SLIP model. The results of this optimization led to five different optimal gaits being found for hopping in air, fluidized media, and at the interface between these fluids. When applying the optimal control policies to a single leg robotic hopper in mixed fluid it was found that the new controller was able to improve its efficiency by 54% over the previous controller. It achieved this by employing a novel "kickback" and retraction maneuver found by the optimizer. This maneuver was found to improve efficiency even in un-optimized controllers when hopping in deep fluid.**

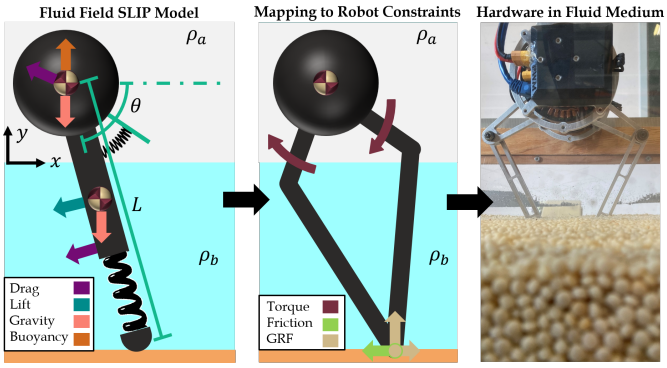

Fig. 1: Mapping from the Fluid Field SLIP model to the Minitaur boom leg.

I. Introduction

Moving through difficult terrain often includes traversing resistive media. Mud, tall grass, sand, snow, and the fluids like air and water that constantly surround living things all have some resistive properties affecting locomotion. Legged systems in laboratory conditions typically only move through air, and ignore resistive media by treating them as a disturbance or noise in the controller. Though these control policies can show impressive robustness [1], [2], the behaviors they choose are likely inefficient or sub-optimal in resistive media. As robots move towards real world implementation, being able to predict and adapt to these dynamic terrain effects becomes increasingly important.

When animals locomote through differing media, they often elect to change their behavior. Humans when running in fluid will generally choose to lift their legs or lean more forward (sometimes called punting) as the fluid depth increases until it becomes more favorable to swim [3], [4]. Similarly, intertidal crabs will choose to use negative touchdown angles with their rear legs to produce efficient thrust in water [5]. Since walking in snow causes the energy expenditures for animals rise [6], humans often change their behavior or use snowshoes to minimize the increased energy cost [7].

Capturing the effect of resistive media (particularly fluids) is highly complex. Models for these behaviors often elect to use high dimensional Partial Differential Equations to capture the pressures, deflections, and vortexes [8] or high dimensional Ordinary Differential Equations to approximate the mass interactions [9], [10]. These models are computationally expensive and require tuning an array of parameters for specific scenarios making them difficult to generalize.

One class of models which alleviates this process are resistive force models. These models simplify the complex fluid dynamics problems by separating them into governing forces and generalized fluid phenomena acting on a body. These have been used recently to capture the dynamics of snake-like motion [11], legged locomotion with the U-SLIP [12], and the Viscous-media SLIP models [13]. The Fluid-Field SLIP model incorporates additional forces beyond that of previous SLIP-like models, and has captured the dynamics of in-air hopping, submerged hopping, and surface swimming [14]. Although resistive models for robot/substrate interaction are simpler, they are complex enough that they have not yet been utilized to power an experimentally verified optimal gait.

Offline optimization techniques ranging from model-based [15] to model-free [16] have historically been used to control legged robots. Model-based trajectory optimization [17], [18] has become an increasingly reliable gait synthesis method. More specifically direct collocation methods [19] cast the evolution of the system dynamics as equality constraints in a nonlinear program. While direct collocation approaches typically use multibody [20], [21], [22] or reduced-order mechanics-based plant models [23], [24], recent work has applied trajectory optimization methods to include models of deformable terrain [25], [26] and slippery surfaces [27]. However, this method has yet to be applied to resistive models of legged locomotion.

In this paper, we apply trajectory optimization techniques on a low parameter model of resistive terrains, the Fluid-Field SLIP model, and generate energy optimal leg control policies.

[1] Florida A&M University-Florida State University
[2] DEVCOM Army Research Laboratory

Leg Boom Parameters			
Parameter	Symbol	Value	Units
Body mass	M	1.36	kg
Leg mass	m_l	0.19	kg
Linear Stiffness	k	1453	N/m
Nominal Leg Length	L_0	23	cm
Proximal leg link length	L_1	10	cm
Distal leg link length	L_2	20	cm
Leg Thickness	W_{Leg}	1.778	cm
Effective Body Radius	R_b	3.4	cm
Environmental/Geometric Parameters			
Gravitational Acceleration	g	9.81	m/s^2
Fluid Depth	Dep	0-15.24	cm
Air Density	ρ_a	1.225	kg/m^3
Bed Density	ρ_w	550	kg/m^3
Static Friction Coefficient	μ_s	0.52	-
Body Drag Coefficient	C_{dB}	0.47	-
Leg Drag Coefficient	C_{dL}	6.4	-
Body Lift Coefficient	C_{lL}	0.001	-
Motor Parameters			
Motor no-load speed	ω_{NL}	157	rad/s
Motor stall torque	τ_{st}	5.92	rad/m
Motor torque constant	K_t	0.075	Nm/A
Motor internal resistance	R_m	0.19	Ω
Optimization Timing Parameters			
Cycle Frequency	ω_{cyc}	2.0-5.5	Hz
Duty Factor	$Duty$	25-85	%
Flight Controller Parameters			
linear P gain	$k_{p,fl}$	726.5	N/m
linear D gain	$k_{d,\zeta,fl}$	$0.2\times\tau_{st}$	Ns/m
Torsional P gain	$k_{p,\psi,fl}$	$1\times\tau_{st}$	Nm/rad
Torsional D gain	$k_{d,\psi,fl}$	$0.04\times\tau_{st}$	Nms/rad

TABLE I: Physical parameters computed for the two degree of freedom leg and used in the trajectory optimization model, including control parameters for flight phase controller (in hardware) and timing (in the model).

We accomplish this by making explicit considerations in our optimization for the unique challenges of hybrid systems in mixed media (i.e. nonlinearities and discontinuities occurring in gradients due to hydrodynamic forces and mixed fluid fields). Next we implement the optimized foot trajectories on a single legged hopper in both air and mixed resistive media. Although the models do not fully capture the interplay of the robot and terrain, they are good enough to generate new gaits that, when implemented on a single leg version of the Minitaur robot [13], have a reduced cost of transport (by more than half) over previous control schemes. Finally, we describe a new behavior that emerges from the optimization for efficient hopping in resistive media: a "kickback" and retraction maneuver.

II. Optimization Methods

The following subsections outline the optimization problem for the chosen resistive model, and the considerations for handling the hybrid system in mixed fluid fields.

A. Dynamic Model

The model used in our optimization is the Fluid Field SLIP model, shown in Fig.1. This model consists of a psuedo-spherical body and a cylindrical leg with internal linear and torsional damped springs. This model expands on the SLIP model by incorporating viscous fluid drag forces on the body, buoyancy forces on the body, drag on the leg, and lift on the leg. In addition, this model makes explicit considerations for changes in dynamics (forces and centers of pressure) which occur when locomoting in multiple fluids of differing densities. Recently, this model has been shown to capture the dynamics of in air hopping, underwater hopping, and surface swimming [14]. The equations of motion for the stance phase are:

$$(M+m_l)\ddot{L} = -F_{dbR} - F_{fld}\sin(\theta) + F_L \tag{1}$$

$$(M+\frac{1}{3}m_l)L^2\ddot{\theta} = F_{db\theta}L + F_{dL}L_{cpd} - \tau_{fld} + \tau_L \tag{2}$$

While the equations for flight are:

$$(M+m_l)\ddot{X} = -(F_{lL}+F_{dL})\sin(\theta) + F_{dbX} \tag{3}$$

$$(M+m_l)\ddot{Y} = F_{fld} + (F_{lL}+F_{dL})\cos(\theta) + F_{dbY} \tag{4}$$

$$\frac{1}{3}m_lL^2\ddot{\theta} = \frac{1}{2}LF_{gL}\cos(\theta) + F_{dL}L_{cpd} + F_{lL}L_{cpl} + \tau_L \tag{5}$$

In the above equations the forces F_{dbR}, $F_{db\theta}$, F_{dbX}, and F_{dbY} are drag forces on the body along the radial, tangential, horizontal and vertical directions respectively, while F_{dL} is the drag force and F_{lL} is the lift force on the leg. Both the leg forces and their respective centers of pressure (L_{cpd}, L_{cpl}) are computed based on pressure integrals along the length of the leg. The net field force (F_{fld}) and its equivalent torque relative to the ground (τ_{fld}) are composed from the gravity force on the leg (F_{gL}), the gravity force on the body, and the buoyant force on the body. The remaining equation parameters and the parameters by which these forces are calculated are expressed in Tables I & II.

Previously this model was controlled by modulating the rest length of these springs in a feed forward sinusoidal motion. Here control is instead performed by directly applying torques and forces on the leg in stance, and torques and leg length in flight. This simplifies the optimization problem as it does not have to ensure the rest length trajectory of the mechanism is continuously differentiable. These rest length trajectories can easily be extracted from the torque and position data in post using numerical integration given known spring stiffness and damping coefficients.

Parameter estimates for this model are found in Table I. The physical parameters of the robot including masses, leg size, and equivalent body radius are taken from robot measurements. Environmental/geometric parameters including leg drag and bed density are taken from previous calculations of the hopper [13] while others are taken from previous work with the Fluid Field SLIP model [14]. The friction coefficient is computed experimentally for a hopper foot on a smooth sheet of ABS plastic. Motor model parameters are taken based on the motor specifications for a U8 T-motor and the lengths of Minitaur's leg. The time variable associated with the optimization is a free parameter used to modulate trajectory timing, but is bounded to ranges previously used by Minitaur hoppers.

B. Design Vector and Timing

The design vector used in the optimization consists of the model states at each collocation node, and two control parameters at each node. During stance, states are composed of the position and velocity of the hip relative to the foot in cylindrical coordinates, and the force and torque the leg is applying on the ground. In flight, the states are composed of the Cartesian positions and velocities of the hip and the angular position and velocity of the leg relative to the hip. In flight the control parameters are leg length and hip torque. This results in a total design vector length, l, of

$$l = 6n_{st} + 8n_{fl} \tag{6}$$

where n_{st} and n_{fl} are the number of collocation points in stance and flight respectively.

The timing differential between collocation points is regulated by two additional non-optimized parameters: cycle frequency and duty factor. The cycle frequency determines the duration of the gait, and thus sets a constant time increment between collocation points. The duty factor is the percentage of time that the stride is in stance.

The initial guess for the design vector is seeded using continuous (but infeasible) trajectories which significantly simplified the expected behaviors of the leg during locomotion. These are guided by insights from our previous experimental study [13]. The guess consists of sinusoidal waveforms retracting and swinging the leg forward in stance and imposing a constant forward motion with a retracted leg in flight.

C. Constraints

Parameter bounds of the design vector for the trajectory optimization are shown in Table II. Leg lengths and angles are bounded by the leg kinematics. Vertical position (defined with respect to the higher fluid surface) are bounded from 1 meter above the fluid to the depth of the rigid substrate. Velocities and the fore-aft position are not explicitly bounded. Forces and Torques are bounded to a moderately conservative range to assist in optimization speed but are primarily bounded implicitly by subsequent constraints.

Additional constraints on the optimization can be broadly categorized into 5 types: collocation constraints, limit cycle constraints, position constraints, force constraints, and robot tuned constraints. Collocation equality constraints consist of estimates of the model dynamics using a Hermite-Simpson approximation from the equations of motion. This method was chosen as it showed a notably higher degree of accuracy (when compared to explicit Euler and trapezoidal estimates of the model) better matching the time marching integration using the ODE45 solver in Matlab. Limit cycle equality constraints consist of coordinate transformations at lift off and touchdown which ensure that the leg touches down at its original configuration and that the configuration end of the stance phase directly maps to the beginning of the flight phase. Additionally these include linear constraints that ensure the leg lifts off with a positive velocity and the net motion is in the forward direction.

Parameter	Symbol	Upper Bound	Lower Bound	Units
Leg length	L	14	30	cm
Leg angle	θ	-135	-45	deg
Flight Fore-aft Pos.	X	-0.3	∞	m
Flight Vertical Pos.	Y	$-Dep$	0.6	m
Leg length Vel.	$\dot{L}$	$-\infty$	∞	m/s
Leg Angular Vel.	$\dot{\theta}$	$-\infty$	∞	deg/s
Flight Fore-aft Vel.	$\dot{X}$	$-\infty$	∞	m/s
Flight Vertical Vel.	$\dot{Y}$	$-\infty$	∞	m/s
Leg Force	F_L	-150	150	N
Leg Torque	τ_L	$-2\tau_{st}$	$2\tau_{st}$	Nm

TABLE II: Optimization design vector utilized algorithm and for direct collocation.

Inequality constraints on foot position and forces are shown below.

$$\begin{bmatrix} Y + Lsin(\theta) \\ -Y - Lsin(\theta) - Dep \\ -F_y \\ -\mu_s F_y + |F_x| \\ |[F_L, \tau_L]J^{-1}|' - |\tau_{st} - \tau_{st}/\omega_{nl} J[\dot{L}, \dot{\theta}]'| \end{bmatrix} \leq 0 \tag{7}$$

The first two inequalities ensure that the foot does pass below the ground or leave the fluid during the flight phase (for reasons explained in the following section). The next two inequalities ensure that the vertical force, F_y, is always pushing on the ground and that the legs horizontal force, F_x, is always lower in magnitude that the static friction force. Additional equality constraints are included that ensure the leg lifts off and touches down when $F_y = 0$. The final inequality constraints bound the forces, torques, angular velocities, and leg velocities to a range achievable by the motor. The J shown in the equation is the Jacobian transformation for the leg kinematics and maps cylindrical coordinates to the motor space.

Two robot-tuned constraints were included due to platform specific quirks. This first constrains the lift off and touchdown length to a nominal leg length L_0. It was found experimentally that gaits with nominal lengths longer than this were less robust. The second of these bounds the leg retraction speed in flight. Through experimentation we found gaits which retract too quickly in flight cause very high motor efforts due to the gains and motor dynamics which are not included in the model. Therefore this value is limited to a quarter of its maximum retraction speed, that is $\dot{L}_{fl} = 0.25 L_1 \omega_{nl}$.

D. Model Optimization Procedure

The nonlinear program was formulated using direct collocation and was solved in Matlab using interior-point method via the *fmincon* constrained minimizer with an objective of minimizing the cost of transport (COT) as defined below:

$$P = \omega\tau + \left(\frac{\tau}{K_t}\right)^2 R_m, \tag{8}$$

$$COT = \frac{P}{(M + m_l)gv}. \tag{9}$$

The power, P, is calculated as the sum of the mechanical power and motor heat losses. The torque, τ, and angular velocity, ω, are defined in motor space and computed from the kinematic Jacobian. The velocity v is computed using the average stride velocity. The optimization was limited to 3500 iterations and 40000 function calls to optimize any given gait.

To improve convergence speed, the algorithm uses predefined gradients for both its objective function and constraints. The gradients for the collocation constraints are computed for a single collocation step ($n \rightarrow n+1$) using Matlab's Jacobian function with the Dirac delta functions (which emerged from the sign function in drag and lift calculations) manually removed. This is converted to a function call and used to construct the full collocation gradient sequentially based on the number of collocation points chosen. All other gradients are derived analytically.

The fluid forces (drag, lift, buoyancy) in the Fluid Field SLIP model are piece-wise continuous between fluid interfaces for both the body and leg. As such, defining a continuously differentiable set of dynamics for the purposes of gradient construction is challenging. Therefore to bound the optimization problem, an explicit mode schedule is defined. For in-air or fully submerged hopping, this is a single stance phase and a single flight phase with both the leg and body fully submerged in a fluid of a single density. For mixed fluid hopping, a single stance phase and a single flight phase are used where the body is fully in air and the leg is always partially submerged between the fluid fields. To encourage broader exploration of the space, constraints on the body do not explicitly enforce it to remain above the fluid however the constraint gradient only reflects the out of fluid case.

Optimizations are performed at a selection of simulated depths: one with the model completely in-air, partially submerged in depths of 5, 10, and 15 cm of higher density fluid, and one where the model is fully submerged in higher density fluid. Trajectories output from the optimization are validated using time marching integration of the dynamics model using Matlab ODE45. 100 collocation points were used for optimization, which improved the accuracy of collocation estimate relative to the time marching model.

III. Platform

Experiments using the optimized trajectories were performed on a single leg hopper attached to a 1.34 m boom arm, restricting motion in the sagital plane. The leg, seen in Fig.2, utilizes a direct-drive parallel 5-bar linkage mechanism with two T-motor U8 brushless DC motors. The nominal length of the leg is constrained to 0.23 m for this study with a virtual linear hip spring of 1453 N/m to mimic the spring dynamics in legged locomotion. The flight phase controller also imposes a virtual spring on the leg torsionally (via a PD controller). These parameters are listed in Table I.

To calculate motor power, Eq. 8, the desired motor torque τ and measured motor angular velocity ω from the Hall Effects motor's absolute encoders are used. To measure horizontal speed, v, an Encoder Outlet model 15s rotary encoder operating in quadrature phase was used. On the boom, data is recorded at 1000 Hz with a Teensy 3.6 microcontroller.

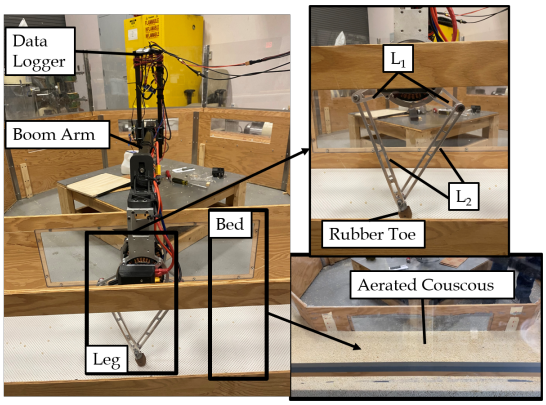

Fig. 2: Coaxial 5-bar single legged hopper attached to a boom and the fluidized bed.

A. Fluidized Bed

To experimentally test gait optimization methods during movement in resistive terrain, fluidized granular media was used as a surrogate for resistive media such as water, mud, and tall grass. To construct a fluidized bed, granular material is placed in a chamber and air is blown up though the granular media. The up-flow of air reduces the hydrostatic loading between grains. At a critical air speed, the up-flow suspends the grains completely and the media is fully fluidized [28]. For this study, a 15 cm deep bed of fluidized couscous was used as the resistive media. A full description of the fluidized bed setup can be found in [13].

B. Control Implementation

To implement the trajectory control on the hardware the torques and forces on the leg are mapped to a time based trajectory of prescribed position.

$$\dot{\theta}_{pre} = \frac{\tau_L + \kappa(\theta - \theta_{pre})}{\beta} + \dot{\theta} \tag{10}$$

$$\dot{L}_{pre} = \frac{F_L + k(L - L_{pre})}{b} + \dot{L} \tag{11}$$

Eq.10 & Eq.11 map the force and torque at each collocation point to continuous desired trajectory points. The linear and torsional stiffnesses of the leg are k and κ while the linear and torsional dampings are b and β, respectively. These equations are numerically integrated using matlabs ode45 command and mapped to a 99 point time based trajectory which is implemented on the robot.

IV. Results and Discussion

Model-based optimizations were performed for 5 cases: in-air, 5cm depth, 10cm depth, 15cm depth, and fully submerged running. Experimental tests for the in-air and 15cm depth cases were then run on the boom hardware. Fully submerged trials could not be run due to track limitations. To determine the

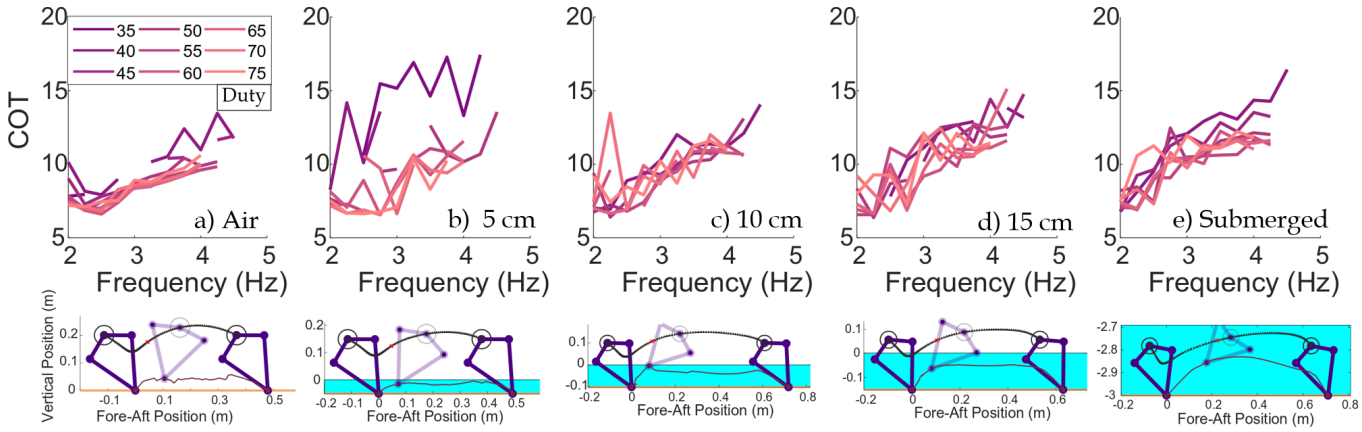

Fig. 3: Coarse parameter variation cycle frequency and duty factor for the model based trajectory optimization showing predicted costs of transport and leg trajectories at the most optimal gaits found in each case.

optima to implement on the hardware a parameter variation of the timing variables: frequency and duty factor was performed.

A. Simulated Results

Optimized trajectory results for the range of frequencies and duty factors considered are shown in Fig.3. For in-air gaits (Fig.3A) it was found the higher frequency gaits generally optimized to a higher COT. Although duty factor was shown to have a direct influence on overall speed of the optima, it did not have a significant effect on the COT outside of the lowest duty factor tested (35%). The leg length did not generally have a pronounced leg retraction during flight preferring to remain close to the nominal leg length. The lowest COT found occurred at 2.5 Hz and at a duty factor of 60%.

The partially submerged fluid cases are shown in Fig.3B-D. Again, the optimized gaits did not show a significant relationship between COT and duty factor except at the most extreme cases (35% & 75%). All tested gaits showed generally increasing costs as the frequency increased and slower speeds than hopping in air. All cases elected to utilize some degree of leg retraction when hopping, with nearly all gaits retreating to the minimal leg length based on the allowable range (fluid depth). The minimum COT is slightly higher for the 5cm gait due to this constraint limiting its retraction ability and jump height. The minimal COTs were found to occur at the a frequency of 2.0Hz and, for the 15cm depth, at a duty factor of 60%.

COT of the submerged gait is shown in Fig.3E. The optimal solutions for fully submerged gaits showed behavioral similarity to the mixed fluid cases. The optimizer chose to quickly reduce the leg length in flight maintaining it for most of the flight phase. When compared to the 15cm depth fluid, optimal running gaits were 12% slower. The average power demand did not significantly change from deepest mixed fluid cases as the increased torques used to push the body forward with a higher drag force were partially offset by the decreased leg force required due to the buoyant effect of the submerged body. Global optimal gaits were again found at low frequencies, both minimized at 2.0 Hz with running at a duty factor of 40% and for punting at a duty factor of 55%.

Generally all behaviors found during optimization, regardless of fluid, chose to minimize the leg length in stance to achieve maximum compression and reduce drag losses when rotating about the substrate. They also showed a smooth stance compression phase and achieved their maximum horizontal speed at the instant of liftoff. Notably, none of the optimizations converged to punting style behaviors suggested by previous models [12], [29] under these fluid parameters (without encouragement via constraints or altering the initial guess). All gaits instead chose running style behaviors.

B. Hardware Results

In the hardware, optimal gaits identified in simulation were tested for the in-air and 15cm mixed fluid cases (which was the deepest tested in previous studies). Resulting foot extension and angular trajectories (both in simulation and for the boom) are shown in Fig.4. For the in-air behavior, foot trajectories showed high correlation between the simulated gaits, with an average deviations of 1.9 cm and 5.1° from simulated from the predicted length and angle. The predicted velocity and COT for this behavior were 1.2 m/s and 6.6 while the boom results showed a velocity of 1.05 m/s COT of 10.65. The higher COT and lower velocity come in part from an early touch down in stance causing high breaking forces which removed energy.

In the mixed fluids it was found that gaits hopped slower than the simulated predictions, at roughly 45% the estimated speed. This, combined with higher than expected requisite torques, increased the COT by up to an order of magnitude with costs of: 39.61 running gait. Extension trajectories followed the simulation with reasonable accuracy with average deviations from the simulated behaviors by 1.2 cm and 1.5 cm. Two likely reasons for the differences between the predicted and actual COT are that the model does not account for the effect of ”added mass” (particularly for retractions) and it does not include increased friction due to incomplete aeration of the couscous.

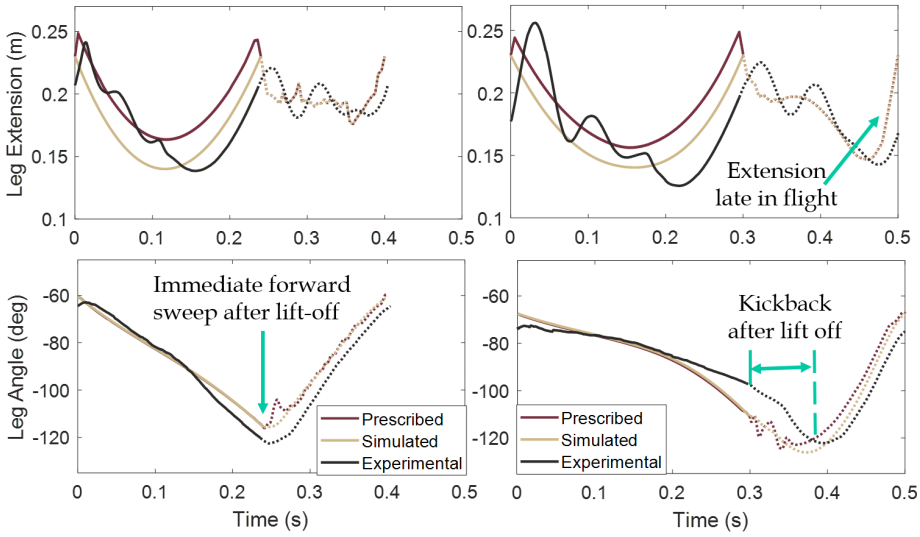

Fig. 4: Comparison of simulated (gold), commanded (garnet), and experimental (black) foot trajectories for optimized behavior in stance (solid) and flight (dashed) for the in-air running, and mixed media running.

Despite these differences, the optimization improved the robot's COT from previous (best) un-optimized results by 54%, from 87.0 to 39.61, for the 15*cm* mixed fluid case. The optimization process, given its increased freedom by which it may shape the trajectory compared to previous controllers, selected foot motions with notable asymmetries in the mixed media. In air, for the simulated optimal gait, the stance extension profile and the leg angular sweep between flight and stance are near symmetric. In the mixed fluid gaits, this is not the case. In the mixed fluid the leg extension begins a little after the second half of stance when the leg is more streamlined in the direction of motion. In these cases the leg also generally delays the leg re-extension until the later half of flight.

Perhaps the most notable feature occurs in the flight phase in mixed media. At the beginning of the flight phase the leg performs a "kickback" and retraction maneuver, which is characterized by optimizer's decision to continue the leg's backwards angular sweep (minimizing the drag) until the leg has been significantly retracted after which point it begins its reset motion. A similar phenomena can be seen in the flight profiles at the other optimized depths in many cases in simulation. These behaviors are in contrast to the in-air motion which finds an immediate forward swing is optimally efficient. These specific behaviors are results which a controller would not likely find unless it has a useful approximation of the dynamics effects of the resistive media on the leg.

C. Utility of Kickback

To further evaluate the efficacy of the kickback maneuver, it was incorporated into the previous un-optimized state based controller. This controller (described in [13]) synthesizes fixed thrust [30] and active energy removal [31] policies in stance to manage impacts and produce the lift off thrust. The flight phase is broken into three stages: a smooth leg retraction and immediate forward swing, a dwell at the minimum leg length ($\frac{2}{3}L_0$), and a final re-extension to the nominal leg length (L_0). To incorporate kickback a smooth sine wave was added in the first stage of flight which modulated the leg angle from its instantaneous lift off angle by a fixed magnitude. After this (during the second stage of flight) the leg would perform its immediate forward swing.

The kickback augmented control was tested in air and at the deepest possible bed depth (20.3*cm*) against the unmodified control. Kickback magnitudes of 10° and 20° were implemented and all trials were run thrice. It was found that at the deepest bed depth kickback notably reduced the COT relative to the unmodified control, by 12% at 10° and 20% at 20°. Moreover, it was found that kickback did not significantly change the COT in air, increasing the average COT by 1.2% at 20° but decreasing the COT by 6.7% at 10°. This suggests that kickback can be added to hopping controllers without accruing significant losses on land while notably improving performance in water.

V. Conclusions and Future Work

To address the challenging problem of developing efficient strategies for legged locomotion in resistive media, we developed a model-based trajectory optimization approach. To generate solutions reliably, we employed a direct collocation formulation applied to the recently developed Fluid Field SLIP model. Explicit considerations were made in the optimization for the unique dynamics of the hybrid system under mixed fluid forces and for the robot on which the optima were planned and tested. Using different fluid depths (from in-air to fully submerged) five optimal behaviors were found. When applied to the hardware, although the optimized behaviors showed lower over all efficiency compared to the simulated estimates, the optimal gaits found improved hopping efficiency in mixed

resistive media by 54% over previous controllers. Much of this can be attributed to the "kickback" retraction maneuver found by the optimizer. When applying this kickback concept to the previous best fluid controller it was found to improve the COT at the most extreme depths by up to 20% without causing significant COT losses in air.

In the future we plan to improve the accuracy of the fluid model for this type of resistive media. In particular, dry/viscous friction and anisotropic added mass are likely causes for the unpredicted losses when moving through couscous. With a more accurate model a comparison will be made between different optimization methods (hardware-in-the-loop and model-based) to determine the most effective way to design reliable control for running through resistive media. Following this we will instantiate on-the-fly adaptations of locomotion through different fluids/media and design effective transitions between them.

ACKNOWLEDGMENT

Research was sponsored by the DEVCOM Army Research Laboratory and was accomplished under Cooperative Agreement Number W911NF-17-S-0003. The views and conclusions contained in this document are those of the authors and should not be interpreted as representing the official policies, either expressed or implied, of the Army Research Laboratory or the U.S. Government. The U.S. Government is authorized to reproduce and distribute reprints for Government purposes notwithstanding any copyright notation herein.

REFERENCES

[1] M. Raibert, K. Blankespoor, G. Nelson, and R. Playter, "Bigdog, the rough-terrain quadruped robot," *IFAC Proceedings Volumes*, vol. 41, no. 2, pp. 10 822–10 825, 2008.

[2] Y. Gong, R. Hartley, X. Da, A. Hereid, O. Harib, J.-K. Huang, and J. Grizzle, "Feedback control of a cassie bipedal robot: Walking, standing, and riding a segway," in *2019 American Control Conference (ACC)*. IEEE, 2019, pp. 4559–4566.

[3] T. Kato, S. Onishi, and K. Kitagawa, "Kinematical analysis of underwater walking and running," *Sports Medicine, Training and Rehabilitation*, vol. 10, no. 3, pp. 165–182, 2001.

[4] G. L. Killgore, A. R. Wilcox, B. L. Caster, and T. R. M. Wood, "A lower-extremities kinematic comparison of deep-water running styles and treadmill running." *Journal of strength and conditioning research*, vol. 20 4, pp. 919–27, 2006.

[5] M. Martinez, R. Full, and M. Koehl, "Underwater punting by an intertidal crab: a novel gait revealed by the kinematics of pedestrian locomotion in air versus water," *Journal of Experimental Biology*, vol. 201, no. 18, pp. 2609–2623, 1998. [Online]. Available: https://jeb.biologists.org/content/201/18/2609

[6] K. L. Parker, C. T. Robbins, and T. A. Hanley, "Energy expenditures for locomotion by mule deer and elk," *The Journal of Wildlife Management*, pp. 474–488, 1984.

[7] R. C. Browning, R. N. Kurtz, and H. Kerherve, "Biomechanics of walking with snowshoes," *Sports biomechanics*, vol. 11, no. 1, pp. 73–84, 2012.

[8] L. J. Fauci, "A computational model of the fluid dynamics of undulatory and flagellar swimming," *American Zoologist*, vol. 36, no. 6, pp. 599–607, 1996.

[9] Y. Jiao, F. Ling, S. Heydari, E. Kanso, N. Heess, and J. Merel, "Learning to swim in potential flow," *Physical Review Fluids*, vol. 6, no. 5, p. 050505, 2021.

[10] J. Dai, H. Faraji, C. Gong, R. L. Hatton, D. I. Goldman, and H. Choset, "Geometric swimming on a granular surface." in *Robotics: Science and Systems*, 2016, pp. 1–7.

[11] E. Hannigan, B. Song, G. Khandate, M. Haas-Heger, J. Yin, and M. Ciocarlie, "Automatic snake gait generation using model predictive control," in *2020 IEEE International Conference on Robotics and Automation (ICRA)*. IEEE, 2020, pp. 5101–5107.

[12] M. Calisti and C. Laschi, "Morphological and control criteria for self-stable underwater hopping," *Bioinspiration & Biomimetics*, vol. 13, no. 1, p. 016001, nov 2017. [Online]. Available: https://doi.org/10.1088%2F1748-3190%2Faa90f6

[13] S. Gart, R. Alicea, W. Gao, J. Pusey, J. Nicholson, and J. E. Clark, "Legged locomotion in resistive terrains," *Bioinspiration & Biomimetics*, dec 2020. [Online]. Available: https://doi.org/10.1088/1748-3190/abd011

[14] M. P. Austin and J. E. Clark, "The fluid field slip model: Terrestrial-aquatic dynamic legged locomotion," in *IEEE International Conference on Robotics and Automation, 2021. Proceedings. ICRA'21. 2021*. IEEE, 2021.

[15] A. Hereid, O. Harib, R. Hartley, Y. Gong, and J. W. Grizzle, "Rapid trajectory optimization using c-frost with illustration on a cassie-series dynamic walking biped," in *2019 IEEE/RSJ International Conference on Intelligent Robots and Systems (IROS)*. IEEE, 2019, pp. 4722–4729.

[16] Z. Xie, P. Clary, J. Dao, P. Morais, J. Hurst, and M. Panne, "Learning locomotion skills for cassie: Iterative design and sim-to-real," in *Conference on Robot Learning*. PMLR, 2020, pp. 317–329.

[17] K. D. Mombaur, R. W. Longman, H. G. Bock, and J. P. Schlöder, "Open-loop stable running," *Robotica*, vol. 23, no. 1, pp. 21–33, 2005.

[18] W. Xi, Y. Yesilevskiy, and C. D. Remy, "Selecting gaits for economical locomotion of legged robots," *The International Journal of Robotics Research*, vol. 35, no. 9, pp. 1140–1154, 2016.

[19] M. Kelly, "An introduction to trajectory optimization: How to do your own direct collocation," *SIAM Review*, vol. 59, no. 4, pp. 849–904, 2017.

[20] I. R. Manchester, U. Mettin, F. Iida, and R. Tedrake, "Stable dynamic walking over uneven terrain," *The International Journal of Robotics Research*, vol. 30, no. 3, pp. 265–279, 2011.

[21] T. L. Brown and J. P. Schmiedeler, "Gait transitions and disturbance response for planar bipeds with reaction wheel actuation," in *2016 IEEE/RSJ International Conference on Intelligent Robots and Systems (IROS)*. IEEE, 2016, pp. 3393–3398.

[22] A. Hereid, C. M. Hubicki, E. A. Cousineau, and A. D. Ames, "Dynamic humanoid locomotion: A scalable formulation for HZD gait optimization," *IEEE Transactions on Robotics*, vol. 34, no. 2, pp. 370–387, 2018.

[23] C. Hubicki, M. Jones, M. Daley, and J. Hurst, "Do limit cycles matter in the long run? stable orbits and sliding-mass dynamics emerge in task-optimal locomotion," in *2015 IEEE International Conference on Robotics and Automation (ICRA)*. IEEE, 2015, pp. 5113–5120.

[24] W. Gao, C. Young, J. Nicholson, C. Hubicki, and J. Clark, "Fast, versatile, and open-loop stable running behaviors with proprioceptive-only sensing using model-based optimization," in *2020 IEEE International Conference on Robotics and Automation (ICRA)*, 2020, pp. 483–489.

[25] C. M. Hubicki, J. J. Aguilar, D. I. Goldman, and A. D. Ames, "Tractable terrain-aware motion planning on granular media: An impulsive jumping study," in *Intelligent Robots and Systems (IROS), 2016 IEEE/RSJ International Conference on*. IEEE, 2016, pp. 3887–3892.

[26] A. H. Chang, C. M. Hubicki, J. J. Aguilar, D. I. Goldman, A. D. Ames, and P. A. Vela, "Learning terrain dynamics: A gaussian process modeling and optimal control adaptation framework applied to robotic jumping," *IEEE Transactions on Control Systems Technology*, 2020.

[27] W.-L. Ma, Y. Or, and A. D. Ames, "Dynamic walking on slippery surfaces: Demonstrating stable bipedal gaits with planned ground slippage," in *2019 International Conference on Robotics and Automation (ICRA)*. IEEE, 2019, pp. 3705–3711.

[28] T. Brzinski and D. Durian, "Characterization of the drag force in an air-moderated granular bed," *Soft Matter*, vol. 6, no. 9, pp. 3038–3043, 2009.

[29] R. Alicea, K. Ladyko, and J. Clark, "Lift your leg: Mechanics of running through fluids," in *2019 International Conference on Robotics and Automation (ICRA)*, May 2019, pp. 7455–7461.

[30] M. H. Raibert, H. B. Brown Jr, and M. Chepponis, "Experiments in balance with a 3d one-legged hopping machine," *The International Journal of Robotics Research*, vol. 3, no. 2, pp. 75–92, 1984.

[31] B. Miller, B. Andrews, and J. E. Clark, "Improved stability of running over unknown rough terrain via prescribed energy removal," in *Experimental Robotics*. Springer, 2014, pp. 375–388.